WIND
ENERGY
SCIENCE
DISCUSSIONS

A review of wind turbine main-bearings: design, operation, modelling, damage mechanisms and fault detection

Edward Hart[1], Benjamin Clarke[2], Gary Nicholas[2], Abbas Kazemi Amiri[1], James Stirling[1], James Carroll[1], Rob Dwyer-Joyce[2], Alasdair McDonald[1], and Hui Long[2]

[1]Wind Energy & Control Centre, Electronic & Electrical Engineering, University of Strathclyde, Glasgow, UK
[2]Department of Mechanical Engineering, University of Sheffield, Sheffield, UK

Correspondence: Edward Hart (edward.hart@strath.ac.uk)

Abstract. This paper presents a review of existing theory and practice relating to main-bearings for wind turbines. The main-bearing performs the critical role of supporting the turbine rotor, with replacements typically requiring its complete removal. The operational conditions and loading for wind turbine main-bearings deviate significantly from those of more conventional power plants and other bearings present in the wind turbine power-train, i.e. those in the gearbox and generator. This work

5   seeks to thoroughly document current main-bearing theory in order to allow for appraisal of existing design and analysis practices, while also seeking to form a solid foundation for future research in this area. The most common main-bearing setups are presented along with standards for bearing selection and rating. Typical loads generated by a wind turbine rotor, and subsequently reacted at the main-bearing, are discussed. This is followed by the related tribological theories of lubrication, wear and associated failure mechanisms. Finally, existing techniques for bearing modeling, fault diagnosis and prognosis relevant to

10 the main-bearing are presented.

1   Introduction

In 2017 Europe installed a record total of 16.8 GW of additional wind power capacity, bringing the net total installed capacity to 168.7 GW (Wind Europe, 2017). Wind energy is therefore playing a key role in the decarbonisation of the power sector, and so also to the effort to avoid catastrophic climate change. In order to ensure the continued success and growth of the wind

15 industry, the economic viability of wind installations must be maintained. Crucial to this is the reliability of wind turbines and their sub-components, an area which overall has received a lot of attention.

   The motivation for this current review is the observation that the wind industry has identified wind turbine main-bearing (WTMB) failures as being a critical issue in terms of increasing wind turbine (WT) reliability and availability. Recently reported figures show that main-bearing (MB) failure rates (over a 20 year lifetime) can be as high as 30% (Hart et al., 2019).

20 Additionally, industry experts at the 2016 WT Drivetrain Reliability Collaborative Workshop (Keller et al., 2016) consistently identified the MB as being the second most important reliability challenge after WT gearboxes in a diverse range of areas, including: MB failure modes, standards and certification, modelling and measurement of internal axial motion, condition monitoring techniques and lubrication. Perhaps surprisingly, given this recent spotlight on MB failures, WTMBs are almost
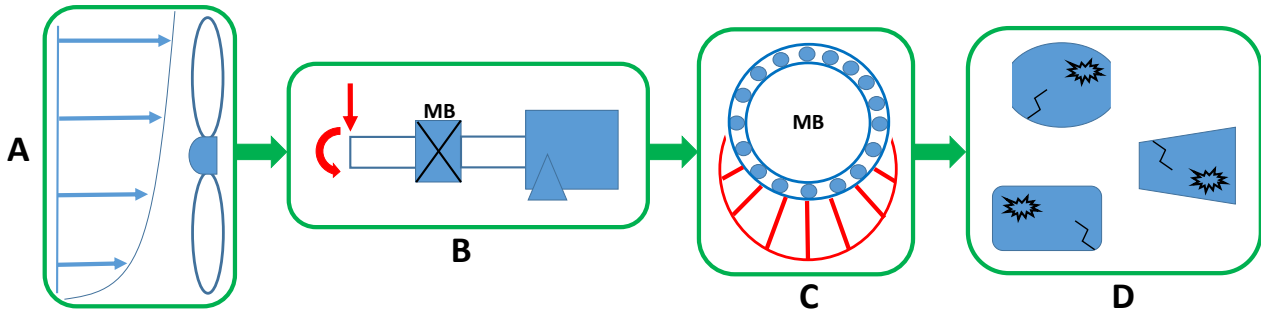
Figure 1. Flow diagram capturing the loading relationships which ultimately lead to main-bearing damage and failure.

completely neglected in the wind energy literature in contrast to other components. This is likely due to the fact that historically the MB has not been reported as resulting in high rates of failure. For example, prominent and often cited reliability studies (Carroll et al., 2016; Hahn et al., 2006; Wilkinson et al., 2011; Spinato et al., 2009) either neglect the MB entirely, or appear to lump it in with other components under the heading of 'Drivetrain', 'Main-shaft' or 'Other', obscuring contributions from

5   the MB itself. These works are often simply reporting the information available to them, and so in turn it seems likely that the MB has not been prioritised in terms of logging failures and considering root cause. This might indicate that MB failures are becoming more of a problem as WTs increase in size, however, there is currently no openly available data with which to test such a hypothesis. As suggested in Hart et al. (2019), there therefore seems to be a significant MB knowledge gap which includes failure data, modelling, measurements and design standards. This is in stark contrast to the hundreds of papers in the

10 literature which consider all aspects of WT gearboxes and generators. The current review seeks to aid the closing of this gap by documenting existing literature which considers, or is relevant to, WTMBs. It is intended that this will form a solid foundation which both motivates and supports much needed future work in this area.

The MB is somewhat of an anomaly in terms of WT drivetrain components owing to the fact that it directly interacts with both the rotor, and associated wind-field dynamics and aerodynamically induced loads, and the other rotating components

15 located further down the drivetrain. As such, the MB sits at an interface between various diverse disciplines, including wind field dynamics, WT operation and control, mechanics and loading of rotating machines and tribological failure mechanisms. The relationship between these various factors which contribute to MB lifetime are captured in Figure 1. At **A**, interactions between the wind field and turbine controller generate loads across the rotor which are then reacted by the MB unit, as shown in **B**. This in turn leads to the internal load conditions experienced by bearing rollers and raceways, shown in **C**, the characteristics

20 of which drive tribological mechanisms which ultimately lead to damage and failure of MB components, shown in **D**. This review will therefore proceed in a manner which mirrors the flow of cause and effect seen in Figure 1, outlining both underlying theory and documented results in order to help facilitate cross disciplinary understanding with respect to these various stages.

Section 2 gives a brief overview of wind turbine technology and outlines the cases under consideration in the current work. Section 3 considers wind field structure, rotor loading and operation and control, i.e. aspects of **A** in Figure 1. Section 4 then

25 outlines the most common choices for MB configuration and rolling elements. The modelling of bearing and roller loads, **B**

and **C** in Figure 1, is presented in Section 5. Section 6 details the tribological mechanisms which lead to MB damage and failure, **D** in Figure 1, and then Section 7 outlines the standards which govern MB design and certification. Finally, Section 8 provides an overview of the existing literature on MB fault diagnosis and prognosis.

2 Wind Turbines

5 While historically there have been various designs for wind turbines, the technology has now standardised to consist almost universally of three bladed horizontal axis machines (Burton et al., 2011). Furthermore, for reasons of improved efficiency and control these machines tend to be variable speed and pitch regulated. The rotational speed is varied, when operating in wind speeds corresponding to below rated power, in order to maintain optimal aerodynamic efficiency. Once rated power is reached, normally at around 12m/s wind speed, the rotational speed is held constant and the blades pitch as wind speeds increase further

10 in order to prevent power and loads exceeding design limits. Drivetrain choices have proved an area for which a consensus on optimal design has not yet been reached, the main split relevant to the current work being between geared and direct-drive (DD) machines. This work will therefore consider both cases for review. There is also a general trend of upscaling for wind turbine installations, with larger machines appearing each year.

3 The Incident Wind Field and Main-Bearing Input Loads

15 The principal role performed by the MB is that of supporting the rotor while reacting non-torque loads, preventing them being transmitted further down the drivetrain. A thorough understanding of WTMB science requires an appreciation of the loading being reacted at the MB. Therefore, the various components which contribute to MB loads, along with their associated characteristics, are presented and discussed in the current section. Incident loads at the MB are those transmitted from the WT rotor to the hub, and then passed through the cantilevered low-speed shaft (LSS) to the MB itself. Loading across the rotor is

20 in turn determined by the structure of the incident wind field. This characterisation of MB input loads therefore begins with a general discussion of wind field structure. Hub loads resulting from rotor interactions with the wind field, and subsequently reacted at the MB via the LSS, are then considered.

3.1 The incident wind field

Wind turbines generate electricity by interacting with the oncoming wind field. These flow fields tend to be turbulent and

25 complex, containing various structures of differing frequency and magnitude, all of which contribute to the loading imparted to the wind turbine and its components. There are many excellent treatises which cover this topic in detail (Mann, 1998; Brand et al., 2011; Stevens and Meneveau, 2017) and so rather than being exhaustive, the present section seeks only to give a general overview of the aspects of this topic which are most relevant to rotor and, therefore, MB loading.

3.1.1 A homogeneous wind field

Ignoring physical effects, such as ground and structural interactions (these will be discussed below), a wind field can be described as a spatially coherent turbulent flow. Turbulence refers to short timescale variations in local wind speed, usually over about ten minutes or less. In order to give a feel for wind field structure, the most common approaches to their being
5   characterised and modelled will be outlined.

The overall wind field is often interpreted as consisting of turbulent fluctuations superimposed onto slower, larger-scale fluctuations such as those related to changing temperatures or weather patterns (Burton et al., 2011). The most common measure of turbulence level is *turbulence intensity*, defined as,

$$I = \frac{\sigma_u}{\overline{u}}, \tag{1}$$

10   where $\overline{u}$ and σ_u are the mean and standard deviations of wind speed measurements, usually over a ten minute period. Spatial coherence, in the wind field definition given above, refers to the fact that wind speeds at points separated in space throughout the wind field are not independent of one another. This is due to wind being a viscous medium, along with the fact that some wind field structures can be fairly large, even with respect to the size of modern wind turbine rotors. The turbulent structure of wind field fluctuations at a point are characterised in frequency space by an autospectral density function, $S_u(n)$, for n a
15   frequency in Hz. The two standard models for $S_u(n)$ are the Kaimal and von Karman spectra (Burton et al., 2011). A coherence function then determines the rate at which correlations between turbulent fluctuations decay as a function of separation, δ, in space. For both spectra mentioned above, coherence models, $C(\delta, n)$, generally take the form of a decaying exponential (Burton et al., 2011),

$$C(\delta, n) = \exp\left(-\delta h(n)\right), \tag{2}$$

20   where $h(n)$ is a monotonically increasing function of n, specified differently for each turbulence model realisation. Mann (Mann, 1998) has also developed a turbulence model using a three dimensional tensor representation of turbulent spectra. This model removes the assumption, implicit for the other two, that the turbulence components in horizontal, lateral and vertical directions are independent of one another. This is mentioned for completeness, for the purposes of the current paper it is a general appreciation of turbulent wind field structure which is of principal importance.

25   ### 3.1.2 Physical Interactions

Wind shear: In reality a wind field will never be perfectly homogeneous, in large part due to the friction interactions of the wind with the non-smooth surface of the earth. This results in a sheared flow, with wind speeds increasing with height. For neutrally stable wind fields it has been shown that wind shear can be well modelled as (Burton et al., 2011),

$$\overline{u}(z) \propto \ln(z/z_0), \tag{3}$$

30   at height z and for roughness length z_0. Roughness length is a parameter which reflects the size of surface asperities at a given site. Its values range from about 0.001 for a flat desert or rough sea, to 0.7m for a city or forest (Burton et al., 2011) . The

relationship is commonly approximated using a power law shear profile,

$$\overline{u}(z) \propto z^{\alpha}. \tag{4}$$

IEC and GL standards (IEC, 2016; GL, 2010, 2012) specify values of α of 0.2 for normal onshore and 0.14 for normal offshore conditions. Although, values of α of up to 0.6 have been recorded (Hart et al., 2016).

5   **Tower shadow** : Additionally to considering the structure of the wind field itself, it is important to consider the impacts of placing a wind turbine into the air flow. With respect to blade and hub loading on a wind turbine rotor, a significant effect is due to tower shadow; this being the blocking effect caused by the tower on the wind flow directly in front of the structure (Dolan and Lehn, 2006). The result is a significant drop in wind speed seen by each blade as it passes the tower. This in turn will impact the dynamic loading across the rotor, and so also the loads incident on the MB.

10   **Yaw error** : Wind turbines can pivot about the tower top in order to ensure the rotor is always facing into the wind. However, it is well known that there are commonly errors in this process, leading to the turbine not facing directly into the wind field (Micallef and Sant, 2016). These yaw errors can result from faulty measurements, bad calibration or simply time lag between the wind changing direction and the turbine following, due to the relatively slow yaw mechanism. From an aerodynamic point of view this results in local wind speeds and blade inflow which change with azimuth angle about the rotor. As with the previous
15   phenomena, this will result in time varying rotor, and so also hub, loads (Micallef and Sant, 2016).

Turbine wakes : A wind turbine produces electricity by extracting energy from the incident wind flow. This manifests itself as a slowing of the wind passing through the rotor as kinetic energy is removed from the flow[1]. The resulting velocity deficit behind the turbine then persists as the flow travels further into the wind farm and this is the wind turbine wake. A turbine wake will slowly expand and recover as it moves further through the wind field due to pressure change and turbulent energy
20   exchange from higher in the flow (Stevens and Meneveau, 2017). However, this recovery process will generally only be partial with respect to standard wind turbine array spacing and depends on various aspects of the wind field such as turbulence levels and atmospheric stability (Stevens and Meneveau, 2017). Subsequent rows of turbines in a wind farm will therefore have inflow which includes superimposed wakes from upstream turbines. The dynamics and modelling of wind turbine wakes and the implications for turbine loading and performance is a vast subject which is still very much under investigation (Archer
25   et al., 2018; Adaramola and Krogstad, 2011).

3.1.3   More complex wind structures

Other structure can be present in a wind field, either caused by more complex physical interactions or inherent to the wind field itself. The former of these includes complex terrain in close proximity to a wind turbine, for example hills, valleys or forests can all significantly altered the flow regime. Inherent wind field structure can also deviate significantly from the standard
30   representations outlined above. Examples of this include: veered flow (a shear like effect where wind *direction* changes with

---

[1]Technically, at the rotor itself it is in fact a pressure energy which is extracted, however, the net effect relevant to the current work is the resulting velocity deficit.
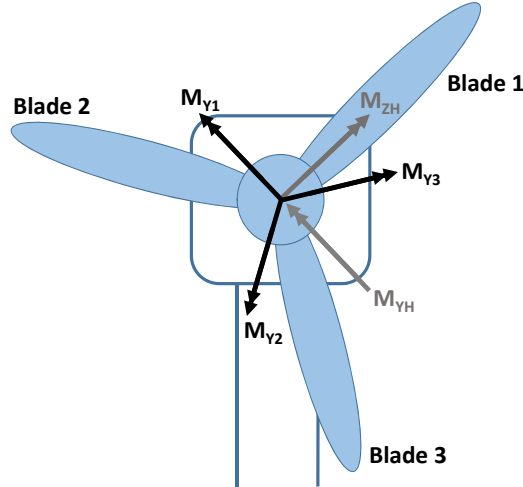
Figure 2. Blade-root and hub moments. The blade-root bending moments are in rotating frames referenced to each blade. Hub moments are in a rotating frame referenced to Blade 1.

height rather than wind speed), coherent turbulence phenomena (Kelley et al., 2005) and low-level jets (Gutierrez et al., 2017, 2014). As with wind turbine wakes, the development of theory to model and relate these phenomena to turbine loading and performance is ongoing.

3.2 Hub loading

5   WT hub loading results from a combination of aerodynamic, gravitational and inertial loads on the rotor (Burton et al., 2011), with a significant contributions coming from rotor weight and blade loading. The forces (as opposed to moments) acting on the hub will be dominated by the rotor weight acting vertically and the thrust force in the downwind direction. In addition, each blade is exposed to both in-plane and out-of-plane loading (with respect to the rotor plane), and so generate moments at the blade root in addition to their force contributions. With respect to a rotating reference frame in which each blade root-moment

10   is expressed with axes set respectively perpendicular and parallel to the given blade, see Figure 2, the resultant out-of-plane moments on the hub can be expressed as follows for a three bladed rotor (Burton et al., 2011),

$$M_{Y_H} = M_{Y_1} - \frac{1}{2}(M_{Y_2} + M_{Y_3}), \tag{5}$$

$$M_{Z_H} = \frac{\sqrt{3}}{2}(M_{Y_3} - M_{Y_2}). \tag{6}$$

15   These equations result from simple trigonometry. Furthermore, rewriting the blade moments as fluctuations about a stationary mean (identical for each blade in a fixed or slowly varying wind profile),

$$M_{Y_i} = \overline{M}_Y + \Delta M_{Y_i}, \tag{7}$$

6

observe that inputting these new expressions into Equations 5 and 6 results in the mean values cancelling, hence the resultant hub moments can be seen to mainly be driven by blade root moment fluctuations about the spatial mean over the rotor circumference.

The aerodynamic blade loads which generate the M_{Y_i} can be decomposed into **deterministic** and **stochastic** components, relating to the physical and turbulent wind field components of Section 3.1 respectively.

3.2.1   Deterministic aerodynamic hub loads

Deterministic aerodynamic loads on the rotor result from rotation in a wind field which varies spatially due to shear profile, tower shadow, yaw error *etc*. The resulting load fluctuations on each blade have a frequency which corresponds to the rotational speed of the turbine, Ω. From the point of view of hub loads in a fixed reference frame, a single rotation sees all blades make a full pass through the wind field, and hence the load frequency for the hub is that of the blades increased by a factor of n, the number of blades. For a 3 bladed turbine the deterministic component of hub load fluctuations therefore corresponds to 3Ω. In this case, deterministic fluctuations in blade root moments, ΔM_{Y_i}, resulting from wind shear and yaw misalignment can often be reasonably well approximated as sinusoids with phase shifts of $0°$, $120°$ and $240°$ respectively (Burton et al., 2011). From Equations 5 and 6 it follows that, in the case of sinusoidal load variations on a 3 bladed turbine, blade root bending moments with range M_{range} result in hub moment fluctuations of $1.5M_{range}$. As above, this result follows via the application of standard trigonometric identities. The very localised variation in blade loads caused by tower shadow will then further increase the load range seen at the hub. Along with 3Ω peaks in the hub load spectra, one would also expect to see associated harmonics of these (6Ω, 9Ω, ...), along with a peak at Ω itself caused by small manufacturing differences between blades. It should be noted that the moment introduced to the turbine shaft from the gravitational force acting at the hub will be opposed by the overturning moment caused by wind shear.

3.2.2   Stochastic aerodynamic hub loads

The wind field itself is non-stationary, turbulent and continually evolving. These wind field variations will therefore lead to variations in the turbine hub loads and moments. Taking moments about an axis parallel to one of the three blades, e.g. M_{Z_H}, the expression for hub moment variance reduces to a double integration across the other two blades and is identical for both M_{Z_H} and M_{Y_H} (Burton et al., 2011). This moment variance is given by (Burton et al., 2011),

$$\sigma_{M_H}^2 = \sigma_u^2 \left(\frac{1}{2}\rho\Omega\frac{dC_L}{d\alpha} \right)^2 \int\limits_{-R}^{R}\int\limits_{-R}^{R} \rho_u^0(r_1, r_2, 0)c(r_1)c(r_2)\frac{\sqrt{3}}{2}r_1\frac{\sqrt{3}}{2}r_2|r_1||r_2|dr_1dr_2, \tag{8}$$

where σ_u^2 is wind speed variance, $\frac{dC_L}{d\alpha}$ the blade lift curve slope, $c(r_i)$ the chord length at the given radius of blade i and ρ_u^0 the normalised cross-correlation function of the wind field. Crucially, this equation demonstrates the dependence of hub moment fluctuations on turbulence, wind field structure and blade aerodynamic design. As in the deterministic case, the interaction of turbine blades with stochastic features in the evolving wind field result in fluctuating loads at a frequency equal to the rotational speed multiplied by blade number, and then also at associated harmonics.
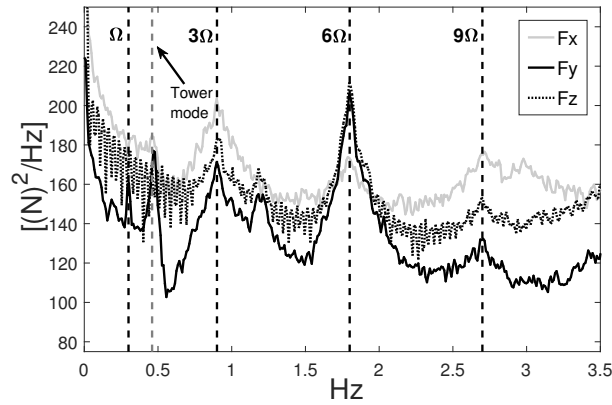
Figure 3. Power spectra of WT hub **forces** in the stationary frame. Prominent peaks can be seen to occur at multiples of 3Ω.
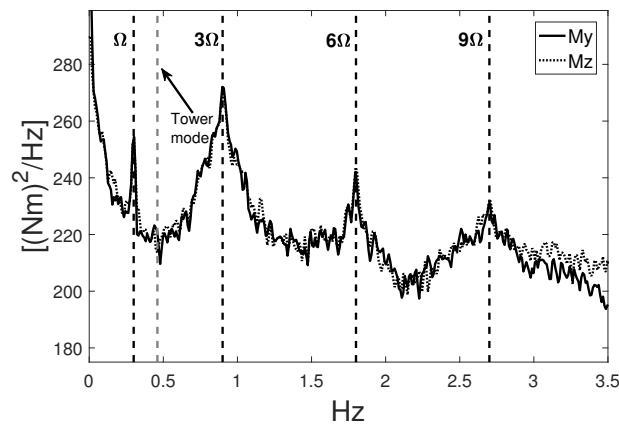

Figure 4. Power spectra of WT hub out-of-plane **moments** in the stationary frame. Prominent peaks can be seen to occur at multiples of 3Ω.

3.2.3 Hub load spectra

In order to illustrate the loads behaviours discussed in the previous sections, example hub load power-spectra (in the stationary frame) are given in Figures 3 and 4. These were generated using data from the simulation of a 3 bladed 2MW wind turbine model in DNV-GL Bladed aeroelastic software. When studying spectra it is important to note that the random nature of stochastic loading will spread the peak out about its central value, hence, sharp peaks stem from deterministic sources and wide peaks from stochastic ones. As discussed, both deterministic and stochastic sources drive loading at multiples of 3Ω for a 3 bladed turbine and so there will be overlap between the different forms of excitation, as can be seen in the figures. Note also some deterministic force loading is present at a frequency which matches the tower natural frequency, and similarly for moments at a frequency that corresponds to rotational speed. Note also that F_x in Figure 3 is thrust force on the hub. Thrust is
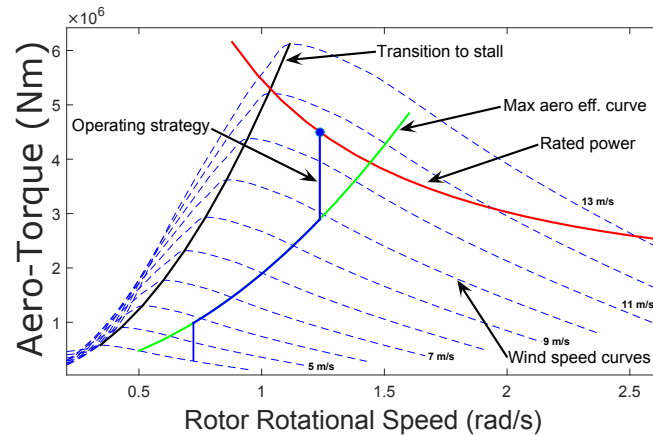
Figure 5. Example torque-speed diagram for a 5MW variable-speed pitch-regulated wind turbine model (Hart, 2018). Pitch control becomes active at the point where the operating strategy reaches the rated power curve.

reacted by the MB along with out-of-plane forces and so a MB experiences continuous variations in both axial and radial loads at these specific frequencies.

3.3 Turbine operation and control

While wind turbine power generation is commonly discussed in terms of above-rated and below-rated conditions, from an
5   operational standpoint each case breaks down into further regions with distinct operational requirements. Figure 5 shows an example design trajectory of a variable-speed pitch-regulated wind turbine as a function of torque and rotational speed. The optimal efficiency tracking region and initial point of pitching can be seen, along with constant speed transition regions. This diagram highlights the fact that there are various regions of wind turbine operation with different design trajectories and associated wind speeds, hence, the load characteristics for the MB will also be different in each case. An additional operating
10   case not seen here is the shutting down of a turbine in above rated conditions when wind speeds consistently stay above a design limit of around 25m/s. Wind turbine operation can additionally include measures to meet certain performance or grid support standards, such as power curtailment or emergency stops. For a detailed discussion of turbine operation and control regions see Hart (2018).

Having outlined various regions/types of wind turbine operation, it is important to note that achieving these operational
15   requirements is then a control task. Like in other industrial applications, wind turbine controllers measure how close to the design trajectory the machine is at a given time and, in cases of deviation, take control action to remove any error. For example, in above rated pitch operation the power is measured and the blades pitched in the appropriate direction if the power is found to be either above or below its rated value. There are many types of wind turbine controller (Novaes Menezes et al., 2018) and each turbine must have a controller tuned to its specific dynamics. As well as following a design trajectory or curtailing the
20   turbine, modern controllers are increasingly required to perform additional tasks such as load alleviation for blades and tower,

the provision of grid frequency support and damping of system resonances (Hart, 2018). These various tasks can be achieved using a range of advanced control techniques including the Power Adjusting Controller (PAC) (Stock, 2015), Individual Pitch Control (IPC) and Individual Blade Control (IBC) (Bossanyi, 2003; Han and Leithead, 2015) among others. Each of these control approaches will alter the behaviour of the turbine with respect to an incident wind field and so in turn will impact the

5   loads seen at the hub and MB. To date there have been no studies which evaluate the impacts of different operation and control approaches to MB loads beyond considering stops and emergency stops (Scott et al., 2012).

As can be seen in Figure 5, the LSS rotational speeds seen by an operating wind turbine are slow, with specific ranges being dependent on size and other design considerations. It is also worth noting that rotational speeds tend to decrease as turbine size increases, this is in order to preserve the optimal ratio between blade tip speed and the incoming wind speed.

10   **4   Main-Bearing Configurations and Rolling Elements**

Wind turbine drivetrains have a number of possible configurations depending on various factors, the most prominent of these being whether the turbine ultilises a gearbox or not. In addition to this consideration, there are loading and cost considerations which drive layout decisions, although of the standard designs there is currently no consensus as to whether one or other is optimal in all cases.

15   Decisions relating to the use, or not, of a gearbox in the wind turbine largely come down to financial factors and trade offs between capital cost, weight, reliability and the OEM's existing expertise. Historically a majority of variable speed wind turbines have used doubly-fed induction generator technology with a multistage gearbox (Polinder et al., 2005). Gearboxes, however, manifest relatively high failure rates and so lost revenue due to down-times and repairs has become a major concern of the wind energy industry (Su et al., 2017; Dabrowski and Natarajan, 2015). New systems have therefore been developed which

20   require gearboxes with fewer stages or are direct-drive (DD), removing the gearbox completely. DD systems are generally more expensive in terms of capital cost due to having large associated dimensions, weight and generators with high torque ratings. However, with no gearbox the component with the highest failure rate has been removed and so these turbines tend to be more reliable than their geared counterparts. As mentioned above, no consensus yet exists as to which generator type is optimal, notably Siemens-Gamesa have committed exclusively to DD technology for all their European offshore turbines in

25   future, whereas Vestas are going with medium and low speed gearbox technology.

4.1   Geared turbines

The most common drivetrain configurations for geared turbines are those with *three-point* or *four-point* suspensions, referring to turbines with either a single (SMB) or double (DMB) main-bearing setup respectively (Guo et al., 2016). Examples of these two configurations are shown in Figure 6, diagrams **A** and **B** respectively. A SMB layout requires gearbox trunnions to

30   react loads at the gearbox end of the LSS and so in combination there are three points of support. This setup has been used in commercial wind turbines by GE, Siemens (prior to becoming Siemens-Gamesa), Nordex and Vestas for machines rated at between 1.5 and 3 MW (Guo et al., 2016). For the DMB layout, a second bearing is placed near the downwind end of the LSS in
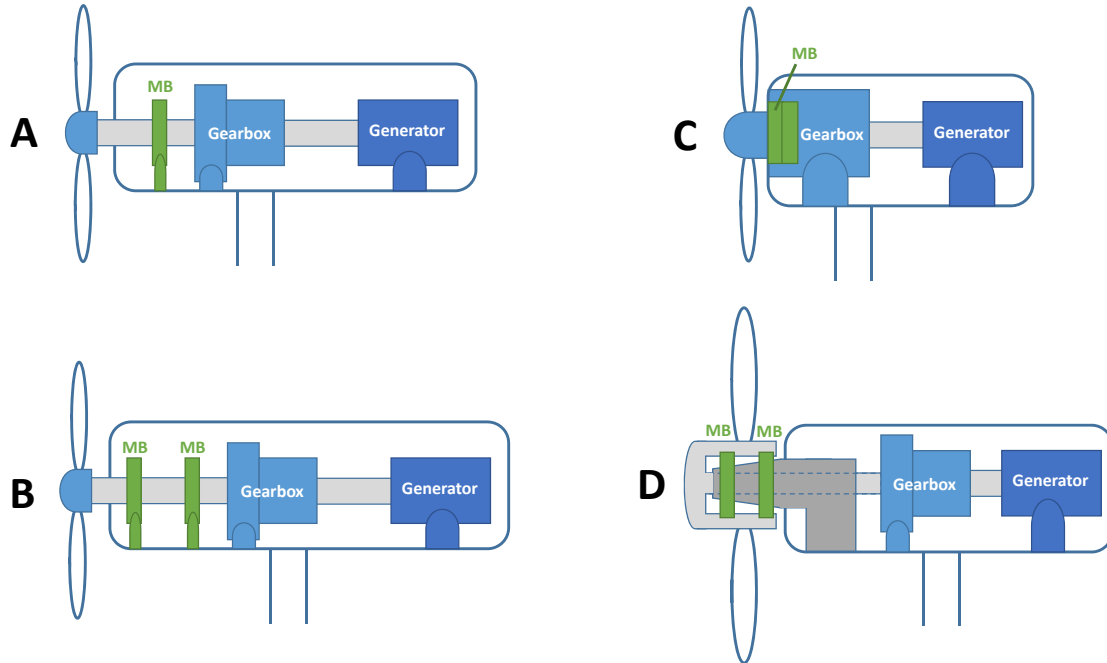
Figure 6. Depictions of the existing drivetrain layouts for geared turbines. In alphabetical order these are: single main-bearing, double main-bearing, gearbox integrated main-bearing and a 'floating drivetrain' design respectively.

an attempt to react non-torque loads before they reach the gearbox. This latter setup has been used in commercial wind turbines by Gamesa (prior to becoming Siemens-Gamesa), Vestas and GE for machines rated at between 2 and 2.5 MW (Guo et al., 2016). DMB designs protect the gearbox more fully from non-torque loads, however, they can be sensitive to misalignment, require more space and have a higher associated capital cost (Bergua et al., 2014; Guo et al., 2016).

5   Designs have also been implemented which integrate the MB directly into the gearbox, removing the need for a main-shaft and so resulting in a very compact overall design. Such a design is shown in Figure 6-**C**. The benefits of such an arrangement lie mainly in the resulting reduction in tower top weight, allowing for cost savings in the WT tower and substructures (Terrell et al., 2012). However, drawbacks have also been identified including: possible early failures due to incompatibilities between the gearbox and remaining nacelle components (to which the gearbox is now a main load path) (Terrell et al., 2012), noise

10   issues from vibro-acoustic propagation and the potential for poor load distributions across gear faces (Bergua et al., 2014). This drivetrain configuration has been used by both Vestas and Areva in 3 and 5 MW wind turbines respectively (Bergua et al., 2014).

Another concept looks to decouple support structure and drivetrain through the implementation of a 'floating drivetrain' design. Two MBs support the rotor as it rotates about a structure fixed directly to the turbine bedplate (Bergua et al., 2014).

15   Torque is then transmitted to the shaft via an elastic coupling towards the front of the turbine hub, as in Figure 6-**D**. The principal drivers for this design are the removal of non-torque loads from being propagated into the gearbox and generator, however,
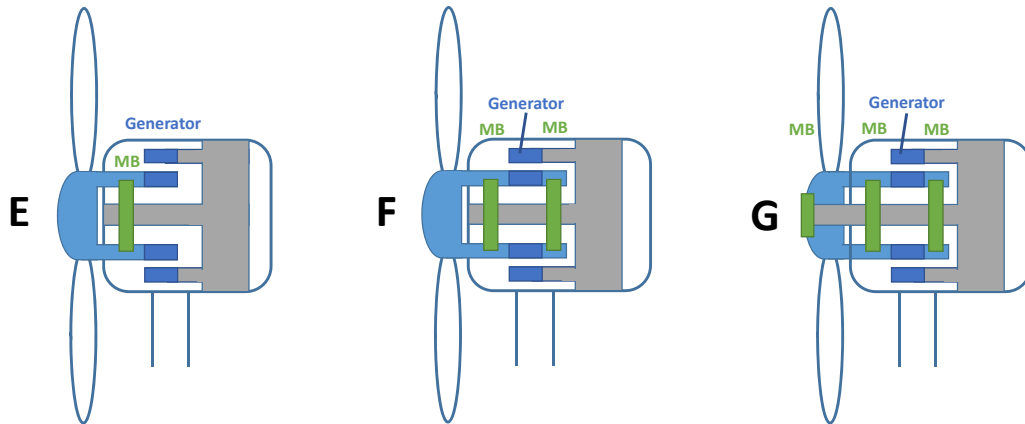
Figure 7. Depictions of some of the existing drivetrain layouts for direct-drive turbines. One example is given for each of single, double and triple MB designs.

load improvements for the MBs themselves are also claimed to result from a more even distribution of loads due to the rotor centre of gravity now presiding between the bearings (Bergua et al., 2014); while this may be the case, no published studies exist which specifically investigate resulting loads on the MBs themselves from such a design although, as will be discussed, this is true in general for all drivetrain layouts. Published figures do show low gearbox failure rates for this drivetrain design

5 (Bergua et al., 2014), but similar figures are not available for the MBs. This design has been used in Alstom turbines for a range of power ratings and will also be used in GE offshore DD installations, as discussed below.

4.2 Direct-drive turbines

Current DD wind turbines are almost all radial flux machines, although axial flux topologies do also exist (Dubois et al., 2000). This work therefore considers the more common radial flux design. Given the integration of support structure and generator

10 in DD turbines, a main design aim becomes ensuring that the specified minimum air-gap clearance is maintained (Stander et al., 2012). This precision task is therefore additionally required of the MBs, along with the transfer of torque and reaction of non-torque loads. Bearings can be arranged in single, double or triple configurations, with various possible layouts in each case (Stander et al., 2012), including having bearings in the air-gap diameter. Figure 7 shows one example of each, for a full accounting see Stander et al. (2012). The 'floating' drivetrain concept introduced for geared turbines can also be applied in DD

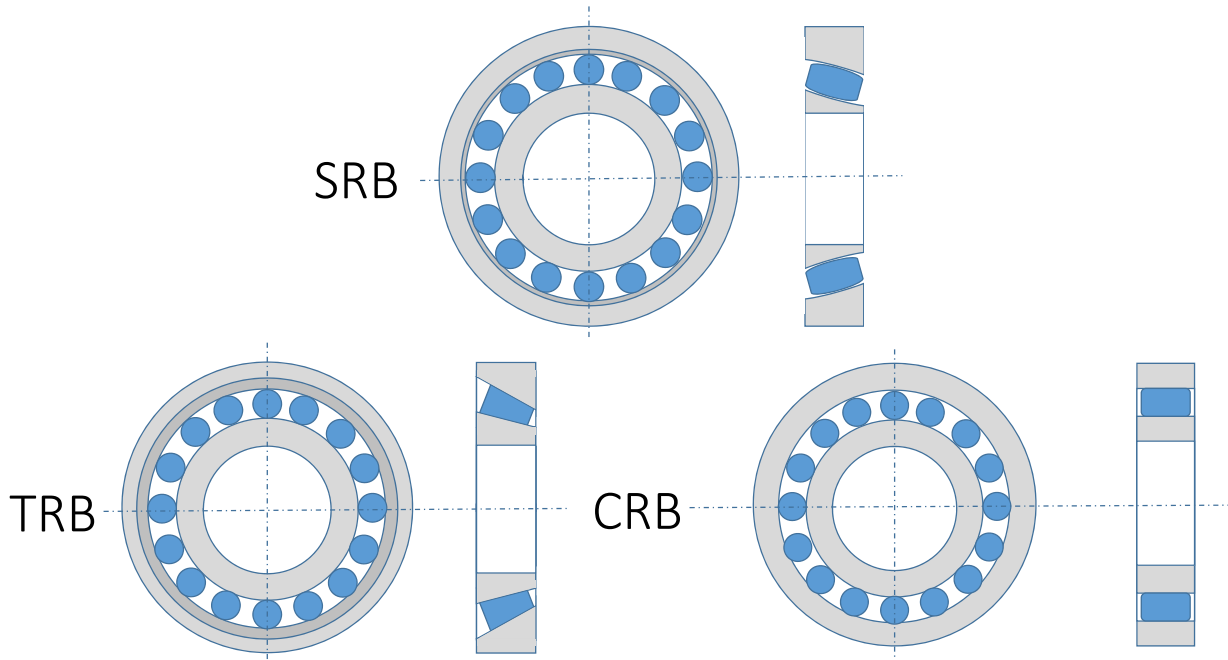15 cases and is currently being used in GE's 6MW offshore wind turbine.

Figure 8. Bearing rolling element types. A single row only is shown for each. Note that for SRBs and TRBs, in WTMB applications, a double row back-to-back configuration will generally be used on the rotor side.

4.3 Rolling elements

The current section gives an overview of the bearing rolling elements used in WTMBs for the various configurations of the previous section. These rolling elements are depicted in Figure 8.

Spherical roller bearings (SRBs): SRBs are characterised by their outer raceway being a portion of a sphere. The rollers, in
5 turn, are shaped such that they conform closely to both inner and outer raceways. This results in a bearing which is internally self-aligning and has a high radial load carrying capacity. A double-row SRB (DSRB) configuration, as in the figure, allows for the reaction of combined axial and radial loading. SRBs cannot support moment loads in either single or double-row configurations (Harris and Kotzalas, 2007).

Tapered roller bearings (TRBs): A single row TRB can carry a combination of axial and radial loads. Differences in contact
10 angles at the inner and outer raceways result in an unbalanced force which will act to drive the roller against its guide flange. The bearing contact angle is determined by the magnitude of axial loading to be reacted, relative to radial loading. As with SRBs, TRBs are commonly put into double-row (or more) configurations (DTRB) in order to increase their radial load carrying capacity. TRBs and DTRBs can support moment loads (Harris and Kotzalas, 2007). Numerical modelling has shown the stiffness and displacement of rollers to be sensitive to the magnitude of applied moment and radial loads (Tong and Hong,
15 2014).

Cylindrical roller bearings (CRBs): CRBs have cylindrical rollers, usually crowned at the ends to prevent high edge stresses. They exhibit low-friction operation compared to SRBs and TRBs and have a high radial load capacity, however, they are unable to support axial loads. Tolerance to small axial loads can be achieved by incorporating a thrust flange into the bearing housing. As previously, a double row (DCRB) may be be used to increase load carrying capacity (Harris and Kotzalas, 2007).

5   **Toroidal roller bearings (TorRBs)**: Similar to SRBs, but with a toroidal outer raceway and elongated rollers by comparison, TorRBs offer an increased radial load carrying capacity while also retaining some of the self-aligning properties of SRBs. TorRBs can only support small axial loads.

As outlined above, WTMBs generally consist of two or more individual bearing units which together support the rotor via multiple suspension points. We now detail which bearings are used in the various cases, along with the specifics of their setups. 10   Two important concepts necessary for this discussion are **locating/non-locating** bearings and **preloading**.

When two or more bearing are being used to support a shaft, in order to prevent excessive axial motion one or both bearings must be fixed in the axial direction. However, changes in temperature during operation (either machine related or due to external influences) will result in thermal expansions which, in the case of two axially fixed bearings, would lead to material stress and deformation. It is therefore generally necessary to have one bearing which is free in the axial direction and so able to 15   accommodate axial displacements (the non-locating bearing), and one which is axially fixed in order to hold the shaft in place (the locating bearing).

Radial preloading of roller bearings is used to increase the number of rolling elements under load around the bearing circumference. This has the effect of reducing the maximum rolling element load and helps prevent skidding[2] (Harris and Kotzalas, 2007).

20   **Geared turbines**: Geared turbines which have either a SMB or DMB setup have historically most commonly used a locating DSRB for the rotor side bearing, along with a SRB, CRB or DTRB as the generator side bearing (Yagi, 2004). The use of SRBs has remained prevalent, along with the introduction of designs featuring two TRBs or a DTRB and CRB (at rotor side and generator side respectively) in the DMB drivetrain case (Yagi and Ninoyu, 2008). More recently, SMB designs which replace the rotor side DSRB with a pre-loaded DTRB or triple-CRB have become available (Fierro, 2017; Schaeffler; Liebherr). 25   Finally, a design also exists for the DMB case which uses a non-locating TorRB and locating DSRB combination (SKF). In the case where the MB is integrated into the turbine gearbox both DTRB and triple-CRB setups have been used (Yagi, 2004; Bergua et al., 2014). The 'floating' drivetrain design uses a spread pair of TRBs for rotor support (Bergua et al., 2014).

Direct-drive turbines: DD turbine mechanical MBs tend to use TRBs, CRBs or TorRBs for rolling elements in either single or double-row formations at each support point of the MB system (Stander et al., 2012). In the case of a SMB with rollers located 30   within the air-gap, disk shaped rollers can be used which are supported by a shaft and small mechanical bearings (Engstrom and Lindgren, 2007).

---

[2]A combination of rolling and sliding.

5   Main Bearing Modeling

As with other aspects of MB theory, there are not many studies which deal specifically with the modelling of WTMBs. However, there is a substantial literature concerned with the modelling of rolling bearings of different types and under various conditions. This section will therefore outline both the existing modelling work concerned with WTMBs, along with relevant contributions

5 from the wider theory which seem likely to play a role in future MB research.

5.1   Hertzian elastic contact theory

Many rolling bearing models are underpinned by Hertz's classical theory of local stress and deformation resulting from two elastic bodies in point or line contact. An excellent overview of this theory can be found in Harris and Kotzalas (2007). The following general load-deflection relationship is obtained from the classical theory,

10 $$Q = K\delta^n, \tag{9}$$

which relates normal contact force, Q, with the radial deflection, δ, at the contact. For a point contact $n = 3/2$ and for a line contact $n = 10/9$. The constant factor, K, represents contact stiffness, and is determined from material properties and the geometry of the contact patch which forms between the bodies. Various analytical approximations have been developed (Antoine et al., 2006; Brewe and Hamrock, 1977) which allow for fast evaluation of the terms necessary for determining contact

15 geometry and K itself with minimal error. Tangential forces due to friction and lubrication conditions are then given by,

$$Q_t = \mu Q, \tag{10}$$

where μ is an equivalent friction coefficient. In the case of roller bearings, the surface will often not be a perfect cylinder and so assuming a line contact can lead to inaccuracies. In order to avoid these errors it has been proposed that the bearing should be partitioned into a number of *slices*, on each of which a perfect line contact is assumed and the forces evaluated as above.

20 The resultant contact force on the entire roller is then a summation, or integration, of those on the slices.

For an applied load resulting in deflection, the point of maximum rolling element load coincides with the point of maximum deflection. Loading at an angle of ψ from the maximum load, $Q_{\max}$, can be evaluated as,

$$Q_\psi = Q_{\max} \left[1 - \frac{1}{2\epsilon} (1 - \cos\psi) \right]^n . \tag{11}$$

The parameter ϵ is related to clearance in the bearing and the radial shift at the centre of the shaft. Its value can be interpreted

25 as giving the proportion of the total bearing circumference which is under load (Harris and Kotzalas, 2007). Figure 1-**C** shows an example radial load distribution for a rolling element bearing with $\epsilon \approx 0.5$. Similar formulations hold for cases of combined axial and radial loading.

5.2   Multibody models

Multibody formulations, modelling the bearing system as a collection of interacting bodies, are most commonly used for

30 bearing models due to their speed and relative simplicity. These models can be quasi-static or dynamic in nature. In both cases,

force expressions are determined which describe loading-deflection relationships between the various bearing components (rollers, races, flanges etc.), with contact loads generally evaluated using the Hertz theory of the previous section. Bearing internal loads and deflections are iteratively solved for, using Newton-Raphson or similar, such that external and bearing forces balance. For the quasi-static case this gives the desired result at each timestep. In the dynamic case, load and stiffness properties

5   from this first stage can be used in a dynamic model to analyze rolling element motion.

Ghalamchi et al. (2013) present a general purpose dynamic SRB model which follows the approach outlined above. Computational efficiency is improved by assuming that: sliding does not occur between bearing components, all rollers move around the raceway with equal velocity and don't interact with each other, isothermal conditions exist throughout. Centrifugal forces acting on the rollers are also neglected. Results from dynamic simulations of both single and double bearing configurations

10 are presented. Both Tong and Hong (2014) and Zheng et al. (2018) develop models to evaluate loading for TRBs subject to combined force and moment loads. The first of these improved upon existing techniques in terms of evaluating pressure distributions along rollers via integration. The latter is specifically considering TRBs for DD floating wind turbine main-shafts and additionally includes effects related to angular misalignment and friction, although cage influences and skew effects are still neglected. Both models are quasi-static in nature. In Jain and Hunt (2011) a dynamic model is derived with which the presence

15 of bearing sliding or skidding (instead of rolling) can be investigated. The model itself is developed for ball-bearings and so would need to be adapted before it can be applied in the MB case, however, given that sliding is associated with some potential MB damage modes (see Section 6) this would seem to be a key point of investigation for future MB research.

The multibody models presented here are all fairly general, mainly differing in terms of considered bearing type and assumptions made during the modelling process. The fundamental building blocks are therefore present for further development

20 of models with which to investigate WTMB loading for different bearing types and configurations. During this development it will be important to appraise the assumptions of the given approaches in order to ensure that the important factors in terms of MB operational loads are accounted for, including a consideration of whether dynamic or quasi-static models are required.

Both SKF and Schaeffler have developed their own multibody simulation softwares for design, testing and optimisation. SKF's software, BEAST (BEAring Simulation Toolbox), can evaluate internal motions and forces in a bearing under specified

25 loads. The model employs an EHL lubrication model and can predict the occurence of phenomena such as wear and fatigue. Schaeffler have developed BEARINX which offers similar features and looks to account for lubricant condition and contamination effects in the model. Another commercially available multibody modelling software, SIMPACK, has been used to analyse MB loads at a number of operating points, while also exploring the effects of bearing clearance (Sethuraman et al., 2015).

5.3 Finite element models

30 Finite Element Methods (FEMs) can be used for modelling of the deformation pressure within a bearing. A function is chosen to represent uniquely the displacement within each node. Then, the element stiffness matrix is obtained from equilibrium and upon obtaining the matrix for the complete bearing, the full matrix is assembled and boundary conditions applied. The solution of the resulting matrix equation produces the nodal displacements (Harris and Kotzalas, 2007). Accuracy of solutions is highly dependent on the number of nodes and so considerable computational power and time is generally required for good results.

Due to its extensive computational time and power required, FEM has mainly been used in bearing applications for modelling of roller-raceway contacts (Jackson and Green, 2005; Zeid and Padovan, 1981). There are however also cases of full bearings being modelled using these methods. For roller-raceway contact modelling, calculations of the distribution and magnitude of surface stresses can be carried out which include the effects of roller and raceway crowning (Harris and Kotzalas, 2007).

5 Results are typically compared with Hertzian calculations for validation. Full bearing modelling has been done to analyse fatigue failure in wind turbine gearbox bearings (Grujicic et al., 2016; Jiang et al., 2015; Lai and Stadler, 2016) and in one case for a WTMB under steady state loads (Liang et al., 2013), and also to understand contact loads within a pitch or yaw bearing (Chen and Wen, 2012). However, no literature currently exists which considers time domain loading of the MB under dynamic operating conditions.

10 Various forms of commercial FEM software are available. Particularly relevant to the wind turbine case is RomaxWIND, developed by Romax Technology and certified by DNV-GL for gear and shaft design analysis.

6 Tribological Theory for Wind Turbine Main-Bearings

Tribology is the science of interacting surfaces in relative motion. As such, it is this discipline which is concerned with the metallurgical effects of roller and raceway interactions in rolling bearings, and subsequent damage and failure mechanisms.

15 The current section seeks to outline the aspects of this theory most relevant to WTMBs.

6.1 Lubrication

Lubrication is the separation and reduction of contact pressure of two sliding or rolling contacts resulting from entrapment of a liquid (or grease) into a converging gap at the contacts (Halme and Andersson, 2010). Separation stems from a hydrodynamic pressure and lubricant film forming between the contacts. The ratio of oil film thickness to local roughness on contacts is

20 denoted λ and determines the mechanism of lubrication. When $\lambda < 1$ (Boundary lubrication) the hydrodynamic action is not strong enough to separate the contact surfaces and loads are mainly carried via solid-solid contact, resulting in increased friction (Halme and Andersson, 2010). Various factors effect the λ value in practise including the availability of oil, bearing surface roughness, elastic deformation of the loaded surfaces and the viscosity and pressure-viscosity relationship of oils. Elastohydrodynamic lubrication (EHL) is a lubrication condition model which takes these various factors into account. In

25 EHL the oil film thickness is slightly higher than the overall contact surface roughness, and so $\lambda > 1$. Importantly, assumed conditions of EHL underpin most bearing life calculations (Halme and Andersson, 2010). Mixed lubrication occurs when $\lambda \approx 1$ and a combination of boundary and EHL regimes are present. When $\lambda \gg 1$ the sliding surfaces are completely separated by a fluid film which is thick in comparison to surface roughness. These conditions only generally occur at less heavily loaded contact interfaces, such as those between a roller and its cage or the roller end and bearing race flange (Halme and Andersson,

30 2010). For WTMBs the specific lubrication regimes at these traditionally moderately loaded contacts have not been investigated directly and hence it is possible that there is divergence from the standard case.

Rolling elements influence the lubricating film layer as they pass. Roller motion ejects oil from the contact area, as does centrifugal action in higher speed applications. Starvation can occur if the oil reflow, back into the raceway, is too slow to replenish the quantity of oil necessary for EHL before the next roller passes (Halme and Andersson, 2010). If a liquid lubricant is used there needs to be some means of ensuring oil flow to contact regions. This can be done through pumping or circulatory

5   splash systems. Grease lubricated bearings are more likely to experience starved conditions as grease is squeezed out of contact regions during roller passage (Halme and Andersson, 2010).

Oil vs Grease Lubrication: Oil lubricants are typically employed for high speed and high temperature applications. They require a system for circulation and, therefore, have higher maintenance demands. However, they are known to work better at cooling the lubricated surfaces. Grease, on the other hand, is thickened oil. Its action allows localization of the lubricant to

10   regions of contact within the bearing. It consists of a suspension of fluid dispersed into a soap or non-soap thickener with the addition of a variety of performance-enhancing additives (Harris and Kotzalas, 2007). Grease is typically used in low speed, low temperature applications. It requires less maintenance due to not requiring a pumping and circulation system, and is typically the lubricant used in WTMBs. Pumping systems do exist for grease re-lubrication, however, these are fairly unconventional and re-greasing is typically done manually, commonly at 6 month intervals for WTMBs.

15   Grease has a more complex, two phase lubrication mechanism, namely the churning and bleeding phases (Lugt, 2016). The churning phase starts when the bearing is lubricated with fresh grease and is distinguished by macroscopic grease flow. After a period of operation (∼24 hours), a large portion of the grease will have been swept to the side of the rolling region. During the churning phase there is a good supply of lubricant and the contacts tend to remain flooded. After the churning phase, macroscopic grease flow stops and the supply of lubricant into contacts takes place through bleeding flow as the grease

20   releases oil through phase separation (Lugt, 2016). When the moving parts of a bearing come into contact with grease, a small quantity of thickened oil will adhere to the bearing surfaces. The oil is then gradually lost through oxidation or evaporation and with time the oil in grease within the contact region will be depleted. The grease lubricant regime is dependant on the balance of lubricant supply and loss mechanisms which determine the film thickness.

6.2   Damage and wear mechanisms

25   This section details the wear and damage mechanisms most likely to effect WTMBs.

6.2.1   Classical fatigue

Dynamic contact conditions generate stress fields and plastic deformation in contacting materials, eventually leading to the formation of fatigue cracks at defects or inclusions in the material structure (Halme and Andersson, 2010). Intersections of such cracks lead to the formation of pits and the releasing of abrasive particles into the bearing environment. Once initiated this

30   process will self propagate through surface roughening, reduced contact areas and increasing levels of abrasive wear. Roller bearing lifetimes, with respect to classical fatigue, can be described statistically as a function of bearing design, load, speed

and lubrication conditions (Halme and Andersson, 2010). The basic formula for the life-rating of a rolling bearing is,

$$L_{10} = \left(\frac{C}{P} \right)^p, \tag{12}$$

where L_{10} is in millions of revolutions, C is the basic dynamic load rating, P the bearing equivalent load and $p = 10/3$ for roller bearings. L_{10} gives the number of revolutions that 90% of a bearing population is expected to survive without experiencing

5 fatigue pit formation (Halme and Andersson, 2010). It is standard practise to modify this basic rating via the multiplication of scalars which account for other factors including speed, oil viscosity, oil contamination or a desired percentile other than 90%. Hence the modified life, L_{nm}, is used which is proportional to L_{10},

$$L_{nm} \propto L_{10}. \tag{13}$$

Implicit to rolling bearing fatigue life prediction, using the above formulations, are certain assumptions which it is important

10 to be aware of. Those most pertinent to the current work are as follows (Halme and Andersson, 2010):

- EHL conditions are assumed to hold throughout the bearing lifetime

- Present theory does not account for intermittent operation, most of the lifetime of a rolling bearing is assumed to occur under steady-state conditions

- These equations do not account for the presence of wear instead of, or as well as, rolling contact fatigue.

15 **6.2.2 Micro-pitting**

Micro-pitting wear has been found to be present in documented cases of WTMB failures to date (Kotzalas and Doll, 2010). Micro-pitting results from an insufficient local lubricant film thickness (potentially resulting from excessive loading or off-design operation) allowing interactions between roller and race surface asperities. In these cases the normal stresses, *i.e.* those accounted for in classical fatigue analysis, are compounded by additional frictional shear stresses. Bulk contact stresses are

20 therefore increased and points of maximum stress move closer to the surface, leading to significant localised stresses beneath asperity contacts and the subsequent formation of micro-pits (Kotzalas and Doll, 2010). Surface asperity interactions associated with this failure mechanism are generally found to occur in situations where there is relative sliding between the contacting surfaces, in addition to the presence of an insufficient lubricant film (Kotzalas and Doll, 2010).

6.2.3 Spalling

25 Spalling is the pitting or flaking away of bearing material, often as a result of some other primary damage mechanism (Timken, 2011). Spalling can occur due to geometric stress concentrations caused by misalignment or excessive loading and by high localised stresses resulting from surface dents and damage or hard particle contamination. Micro-pitting will commonly lead to spalling damage of the effected surface (Kotzalas and Doll, 2010).

6.2.4 Smearing

Smearing is a form of adhesive wear which occurs under sliding contact between two surfaces, involving the transfer of material from one surface to the other. In rolling element bearings this is known to occur in cases where roller rotational speeds change rapidly, for example when a roller accelerates on entering a more highly loaded bearing region (Evans et al., 2013).

6.2.5 Abrasive wear and debris damage

The entrainment of hard particles into bearing contacts can lead to physical damage; either from indentations left by rolling particles, or surface scratching due to sliding particles (Nilsson et al., 2006). Similarly, particles in the lubricant, through contamination or abrasive damage of bearing surfaces, can lead to high local stress fields and abrasive conditions which can be worse than those seen in boundary lubricated regimes. Ductile metallic debris in the lubricant can be rolled over and flattened by rolling elements, leaving larger shallow smooth dents. Brittle materials, such as sand, fractures when rolled over and leaves many small but steep sided dents. Debris damage of these types can lead to fatigue crack formation and spalling (Nelias and Ville, 1999; Ai, 2001). The presence of more brittle particulate contamination can lead to abrasive wear and gradual increases in bearing clearance (Nilsson et al., 2006; Dwyer-Joyce, 1999).

6.2.6 Fretting

Fretting corrosion occurs at interfaces where loads are transferred under oscillating contact micromovements (ISO, 2017b), commonly a result of vibrations in the system. A WTMB may be exposed to both blade and gearbox vibrations and so this type of damage is possible (Yagi, 2004). Prevention of this type of damage involves trying to optimise bearing clearances and lubricant type.

From the above descriptions it should be clear that most of these damage mechanisms are self perpetuating, generally leading to increasing amounts of similar damage. Furthermore, the presence of one can result in the initiation of others, for example: micro-pitting → spalling → abrasive wear.

7 Design standards

There are several ISO standards which underpin wind turbine bearing design specifications. ISO 76 (ISO, 2017a) deals with static load ratings of conventional rolling element bearings. This covers conventional design regarding the shape of rolling contact surfaces and assumes double row bearings to be symmetrical. ISO 76 states that it is not satisfactory in applications where:

- there is considerable truncation[3] of contact area between rolling elements and raceways

---

[3]Truncation is where element-raceway contact moves to the edge of the raceway, resulting in edge stresses, a smaller contact area and overall increased contact pressure.

- application conditions cause deviations from a normal load distribution in the bearing. This can be due to preload, large clearance and surface treatments or coatings.

Bearings are generally designed to avoid truncation but occurrence can cause large reduction in MB life through acceleration of many of the above damage mechanisms. Since time-varying loads and large moments are present in the WTMB case, it

5 is possible that these effects are present for wind turbines. ISO 281 (ISO, 2007) deals with dynamic load ratings and rated life calculations for conventional roller bearings where life is predominantly dependent on rolling contact fatigue. The same limitations apply as those noted above for ISO 76. In addition to this, the life calculations in ISO 281 do not account for the influence of wear, corrosion or electrical errosion (ISO, 2007). ISO/TS 16281 (ISO, 2008) then allows for effects resulting from tilting, misalignment, clearances and internal load differences to be accounted for in rolling contact fatigue life calculations.

10 The above ISO standards form the basis for bearing design and certification in the turbine specific standards by the IEC and DNV-GL. Both the IEC (IEC, 2016, 2013) and GL (GL, 2010, 2012) standards for wind turbines require the use of ISOs 76 and 281 in combination with simulated loads across various operational cases. Additionally, both IEC and GL standards reference ISO/TS 16281. While in both cases the gearbox is given its own section, the MB is not considered specifically in either set of standards. Furthermore, MB design and rolling element selection is made based on fatigue life and static load ratings only.

15 Design implications with respect to the likelihood of other possible damage mechanisms, i.e. those presented in the previous section, are not considered beyond potential adjustments to the modified life L_{nm}.

8 Fault Diagnosis and Prognosis

Rotating bearing monitoring is commonly done through the analysis of vibration signals using either vibration acceleration (VA) measurements or acoustic emissions (AE). These signals can then be analysed in either the time or frequency domain.

20 Commonly, a set of so called *characteristic features* - such as signal RMS value, frequency component amplitudes or statistical moments - are extracted which are then used to relate the signal to previous operating data or known fault cases. When a rolling element passes a local defect on the race surface an impulse is generated which will then repeat as further passes are made. The frequencies of these events are dependent on bearing geometry, rotational speed and the location of the defect. Similarly, a defect on a bearing roller generate impulses as it moves around the bearing circumference which can be detected. The majority

25 of VA and AE methods which have been developed work well in high speed applications. However, as discussed previously, WTMBs are components which operate at low-speeds and high-loads. This has the effect of making them less sensitive to vibrations as a result to defects or damage within the bearing. Therefore, many of the techniques which work well in high speed and moderately loaded cases have been found to be unreliable in this case. Defect identification challenges resulting from the lower speed of the MB may be partially mitigated by recording longer sampling periods of vibration data. For example, a ten

30 second data acquisition period has been found to be less successful in detecting low speed bearing defects than for high speed bearing/gear tooth defects (Carroll et al., 2019). This suggests that one cause of reduced detection rates for faults in low speed bearings may therefore be due to insufficient sampling periods. Some techniques have been proposed for MB fault detection

which use vibration signals; as will be outlined, these techniques tend to also require additional measurements related to the turbine's operation.

In Qu et al. (2011) a MB fault diagnosis technique is proposed whereby stress waves measured in the MB are decomposed using wavelet analysis. It is suggested that faulty vs healthy cases can be classified according to their D_3 and D_4 signals. This work is based on a finite element model of a MB under the assumption that the bearing housing is rigid. Practicalities of how such measurements should be obtained in practise are not discussed. Further work, including real world testing and measurement technique consideration, would be necessary before this method became practicable. Zimroz et al. (2012) looks to diagnose a MB fault by processing signals of peak-to-peak vibration accelerations and turbine power. Real turbine data is used which covers operation with a faulty MB and operation after replacement with a non-faulty MB. Data from rated power operation and close to start-up are filtered out. The proposed method is then to perform a straight line fit to power vs peak-to-peak values, and it is shown that for the given fault example the resulting fit to 'good' data lies below that of 'bad' data. While this is indeed true for the fault example given, the fact that it is the only example makes it difficult to evaluate whether these results hold in general. Furthermore, for such a method to be usable it would be necessary to determine how different two fits need to be to signal that a fault is indeed present. Overlaps in the data from both cases make this task harder and a large number of datasets, including both healthy and faulty MBs, would be needed to properly assess its applicability and robustness. Ghane et al. (2016) propose the use of main shaft VA measurements to detect possible defects in the downwind MB of a DMB drivetrain. MB damage is modelled as a change in stiffness of the locating bearing unit in the axial direction. A cumulative sum method is used to process acceleration signals and indicate when the probability of a change having happened is high enough to trigger a fault warning. A threshold is set which trades off between speed of detection and the likelihood of a false alarm. The data used in the study is obtained via simulation of a 5MW floating turbine in conjunction with a multibody gearbox model. In Hamadache and Lee (2016), a fault detection approach is presented based on shaft-speed measurements. Vibration frequencies introduced to the system (by various types of bearing fault) are known to manifest themselves in the generator stator current. This in turn impacts generator torque and rotational speed. In steady state conditions, the impact of this can be modelled as introducing sinusoidal fluctuations in rotational speed, along with some noise. It is proposed that the detection of these sinusoidal components can warn of a fault being present, while the associated frequencies can indicate the location of said fault. It should be noted that this approach assumes steady-state operation and a fixed torque at the generator. Absolute Value Principal Component Analysis is used as the detection method. Test cases are presented using simulated data with bearing faults represented by the aforementioned rotational speed variations, including a realistic wind speed input time history. The method behaves well for the example data, however, whether or not the various faults manifest themselves as assumed, while also being detectable from real system measurements, is an open question. Finally, although in test cases the method was found to work while in non-steady operation, given that steady-state operation is assumed, it is not clear whether a similar performance would be seen across a turbine's whole operating envelope. Similar approaches to MB fault diagnosis have been proposed which also look to exploit the presence of these same vibration frequencies in the case of a MB fault. For DD bearings Teng et al. (2016) and Wang et al. (2017) do this by way of decomposing vibrations signals using a multiscale enveloping spectrogram and multiscale filtering spectrum respectively; Gong and Qiao (2013) develop an approach which

looks for relevant frequencies appearing in stator current signals using a rotational-speed invariant PSD algorithm. These latter three techniques explicitly account for varying rotational speeds during operation. Zhang (2018) documents an approach to MB fault prediction based on turbine SCADA measurements. An Artificial Neural Network (ANN) is used to determine a normal behaviour model of MB temperature at timestep t as related to MB temperature at time $t-1$ and rotational speed, active

5   power and ambient temperature at timesteps t and $t-1$. Having trained the ANN on 6 months of normal operational data, deviations between predicted and measured outputs of MB temperature are used to warn of faults. False positives are avoided by considering the percentage of time for which warnings are present over a week of operation, with an alarm threshold of 25%. Successful fault prediction on real turbine data is shown for 4 available fault cases from an operational wind farm. For the considered fault cases, the lead times on alarm activation are between 2.5 months and 3 days before failure.

10 ## 9   Discussion

This paper has given a broad overview of the existing theory and literature about, or relevant to, WTMBs. Aspects ranging from wind field structure all the way down to material degradation and damage have been considered in order to account for the full range of interactions necessary for a complete picture of MB loading and lifetime. This also allows for cross-disciplinary understandings to be facilitated since, as has been shown, WTMBs must be considered as sitting at the interfaces connecting a

15 number of disciplines.

The main conclusion which can be drawn from this literature survey is that much future work is required in order for WTMBs to be properly understood. It is clear that the MB has been neglected in terms of both design standards and research focus. This is understandable given the lack of information properly detailing MB failures in terms of frequency and damage modes. With respect to future efforts in this area, failure data concerning MBs (**D** in Figure 1) is therefore of the utmost

20 importance. Knowledge of the types of damage occurring in the field are needed to drive research directions with respect to both numerical modelling and experimental analyses. Equally crucial to this topic is the development of a proper understanding and characterisation of MB loads, *i.e.* hub and LSS loading and subsequent load distributions about bearing circumferences (**A** to **C** in Figure 1). This includes wind field effects, controller interactions and design implications for time-varying loads. Understanding these factors will allow for a proper appraisal of current design standards (the underlying assumptions for which seem to be dubious at best in the MB case) and recommendations for improved design practises. A detailed understanding of

25 how these various factors influence MB loads and lifetimes will also indicate potential solutions. For example, it could be the case that detrimental and damaging MB loads can be easily alleviated through controller design, equally, MB design considerations may in fact hold the key to lifetime extension for these components. Likely, a combination of approaches will be necessary. Finally, while a critical mass of existing MB research has taken place in the areas of detection and prognosis for

30 MB faults, existing methods have been fairly generic and not specific to WTMBs. Therefore, a better understanding of load-damage relationships and prevalent failure modes for operating WTMBs could allow for more tailored approaches to failure detection and prognosis. This could well lead to improved results compared to the, already promising, work which has been done in this area to date.

10 Conclusion

This paper has reviewed existing literature and theory relevant to WTMBs in terms of design, operation, modelling, damage mechanisms and fault detection. The lack of research performed to date which focuses on MBs in wind turbines was high-lighted. Work in the literature relating to wind field structure and resultant loads at the WT hub, subsequently reacted at the

5   MB, was presented. Common configurations and rolling elements for WTMBs were discussed with respect to both geared and DD turbines. The most common approaches to bearing modelling and analysis, falling into dynamic and quasi-static categories, were then outlined. After this, the tribology of rolling bearings and an overview of relevant damage mechanisms was presented. Finally, existing work in the literature which considers the diagnosis and prognosis of WTMB faults was summarised. The pa-per closed with a discussion of the most important next steps for research in this area, with key requirements being a need for

10   detailed WTMB failure data and the development of a proper understanding of WTMB operational loading.

Competing interests. The authors declare that they have no conflicts of interest.

References

Adaramola, M. S. and Krogstad, P. Å.: Experimental investigation of wake effects on wind turbine performance, Renewable Energy, 36, 2078–2086, https://doi.org/10.1016/j.renene.2011.01.024, http://dx.doi.org/10.1016/j.renene.2011.01.024, 2011.

Ai, X.: Effect of debris contamination on the fatigue life of roller bearings, Journal of Engineering Tribology, 215, 563–575, https://doi.org/10.1243/1359659911543808, 2001.

Antoine, J.-F., Visa, C., Sauvey, C., and Abba, G.: Approximate analytical model for hertzian elliptical contact problems, Journal of Tribology, 128, 660, https://doi.org/10.1115/1.2197850, http://tribology.asmedigitalcollection.asme.org/article.aspx?articleid=1467593, 2006.

Archer, C. L., Vasel-Be-Hagh, A., Yan, C., Wu, S., Pan, Y., Brodie, J. F., and Maguire, A. E.: Review and evaluation of wake loss models for wind energy applications, Applied Energy, 226, 1187–1207, https://doi.org/10.1016/j.apenergy.2018.05.085, https://doi.org/10.1016/j.apenergy.2018.05.085, 2018.

Bergua, R., Jove, J., and Javier, E.: Pure torque drivetrain design: a proven solution for increasing the wind turbine reliability, Brazil Windpower 2014 conference and exhibition, 2014.

Bossanyi, E. A.: Individual blade pitch control for load reduction, Wind Energy, 6, 119–128, https://doi.org/10.1002/we.76, 2003.

Brand, A. J., Peinke, J., and Mann, J.: Turbulence and wind turbines, Journal of Physics: Conference Series, 318, https://doi.org/10.1088/1742-6596/318/7/072005, 2011.

Brewe, D. and Hamrock, B.: Simplified solution for elliptical-contact deformation between two elastic solids, Journal of Lubrication Technology, 99, 1977.

Burton, T., Jenkins, N., Sharpe, D., and Bossanyi, E.: Wind energy handbook, Wiley, 2nd edn., 2011.

Carroll, J., McDonald, A., and McMillan, D.: Failure rate, repair time and unscheduled O&M cost analysis of offshore wind turbines, Wind Energy, 19, 1107–1119, https://doi.org/10.1002/we.1887, http://doi.wiley.com/10.1002/we.1887, 2016.

Carroll, J., Koukoura, S., McDonald, A., Charalambous, A., Weiss, S., and McArthur, S.: Wind turbine gearbox failure and remaining useful life prediction using machine learning techniques, Wiley Wind Energ., 22, 360–375, https://doi.org/10.1002/we.2290, 2019.

Chen, G. and Wen, J.: Load performance of large-scale rolling bearings with supporting structure in wind turbines, Journal of Tribology, 134, https://doi.org/10.1115/1.4007349, 2012.

Dabrowski, D. and Natarajan, A.: Assessment of gearbox operational loads and reliability under high mean wind speeds, Energy Procedia, 80, 38–46, https://doi.org/10.1016/j.egypro.2015.11.404, 2015.

Dolan, D. and Lehn, P.: Simulation model of wind turbine 3P torque oscillations due to wind shear and tower shadow, IEEE Transactions on Energy Conversion, 21, 717–724, https://doi.org/10.1109/TEC.2006.874211, http://ieeexplore.ieee.org/document/1677662/, 2006.

Dubois, M. R., Polinder, H., and Ferreira, J. A.: Comparison of generator topologies for direct-drive wind turbines, Proceedings of the Nordic Countries Power & Industrial Electronics Conference (NORPIE), pp. 22–26, http://scholar.google.com/scholar?hl=en{&}btnG=Search{&}q=intitle:Comparison+of+generator+topologies+for+direct-+drive+wind+turbines+including+structural+mass{#}0, 2000.

Dwyer-Joyce, R. S.: Predicting the abrasive wear of ball bearings by lubricant debris, Wear, 233-235, 692–701, 1999.

Engstrom, S. and Lindgren, S.: Design of NewGen direct drive generator for demonstration in a 3.5 MW wind turbine, EWEC (European Wind Energy Conference & Exhibition), Milan, Italy, May 7-10, http://proceedings.ewea.org/ewec2007/allfiles2/137{_}Ewec2007fullpaper.pdf, 2007.

Evans, R. D., Barr, T. A., Houpert, L., and Boyd, S. V.: Prevention of smearing damage in cylindrical roller bearings, Tribology Transactions, 56, 703–716, https://doi.org/10.1080/10402004.2013.788236, 2013.

Fierro, A. J.: Improving bearing life in wind turbine main shafts and gearboxes, Tech. rep., Timken, 2017.

Ghalamchi, B., Sopanen, J., and Mikkola, A.: Simple and versatile dynamic model of spherical roller bearing, International Journal of Rotating Machinery, https://doi.org/10.1155/2013/567542, 2013.

Ghane, M., Nejad, A. R., Blanke, M., Gao, Z., and Moan, T.: Statistical fault diagnosis of wind turbine drivetrain applied to a 5MW floating wind turbine, Journal of Physics: Conference Series, 753, https://doi.org/10.1088/1742-6596/753/5/052017, 2016.

GL: Guideline for the certification of wind turbines, 2010.

GL: Guideline for the certification of offshore wind turbines, 2012.

Gong, X. and Qiao, W.: Bearing fault diagnosis for direct-drive wind turbines via current-demodulated signals, IEEE Transactions on Industrial Electronics, 60, 3419–3428, https://doi.org/10.1109/TIE.2013.2238871, 2013.

Grujicic, M., Ramaswami, S., Yavari, R., Galagalikar, R., Chenna, V., and Snipes, J.: Multiphysics computational analysis of white-etch cracking failure mode in wind turbine gearbox bearings, Proc IMechE Part L:J Materials: Design and Applications, 2016.

Guo, Y., Parsons, T., Dykes, K., and King, R. N.: A systems engineering analysis of three-point and four-point wind turbine drivetrain configurations, Wind Energy, 20, 537–550, https://doi.org/10.1002/we.2022, 2016.

Gutierrez, W., Araya, G., Basu, S., Ruiz-Columbie, A., and Castillo, L.: Toward understanding low level jet climatology over west Texas and its impact on wind energy, Journal of Physics: Conference Series, 524, https://doi.org/10.1088/1742-6596/524/1/012008, 2014.

Gutierrez, W., Ruiz-Columbie, A., Tutkun, M., and Castillo, L.: Impacts of the low-level jet's negative wind shear on the wind turbine, Wind Energ. Sci, 25194, 533–545, https://doi.org/10.5194/wes-2-533-2017, https://www.wind-energ-sci.net/2/533/2017/wes-2-533-2017.pdf, 2017.

Hahn, B., Durstewitz, M., and Rohrig, K.: ISET: Reliability of wind turbines - experiences of 15 years with 1500 WTs, Tech. rep., https://doi.org/10.1007/978-3-540-33866-6, http://link.springer.com/content/pdf/10.1007/978-3-540-33866-6{_}62.pdf, 2006.

Halme, J. and Andersson, P.: Rolling contact fatigue and wear fundamentals for rolling bearing diagnostics - state of the art, Proceedings of the Institution of Mechanical Engineers, Part J: Journal of Engineering Tribology, 224, 377–393, https://doi.org/10.1243/13506501JET656, 2010.

Hamadache, M. and Lee, D.: Wind turbine main bearing fault detection via shaft speed signal analysis under constant load, International Conference on Control, Automation and Systems, pp. 1579–1584, 2016.

Han, Y. and Leithead, W. E.: Comparison of individual blade control and individual pitch control for wind turbine load reduction, EWEA, 2015.

Harris, T. and Kotzalas, M.: Essential concepts of bearing technology, Taylor and Francis, fifth edn., 2007.

Hart, E.: Wind turbine dynamics identification using Gaussian process machine learning, Ph.D. thesis, University of Strathclyde, 2018.

Hart, E., Keegan, M., and McMillan, D.: A lookup table approach to determining wind turbine operational fatigue loading from wind field measurements, ASRANet International Conference on Offshore Renewable Energy, 2016.

Hart, E., Turnbull, A., Feuchtwang, J., McMillan, D., Golysheva, E., and Elliott, R.: Wind turbine main-bearing loading and wind field characteristics (submitted March 2018, revised Nov 2018, awaiting final acceptance), Wiley Wind Energy, 2019.

IEC: 61400-4:2012 Wind turbines part 4: design requirements for wind turbine gearboxes, 2013.

IEC: 61400-1:2005+A1:2010 Wind turbines part 1: design requirements, https://doi.org/10.1007/978-3-642-27151-9, 2016.

ISO: 281: Rolling bearings - dynamic load rating and rating life, 2007.

ISO: TS 16281:2008 Rolling bearings - methods for calculating the modified reference rating life for universally loaded bearings, 2008.

ISO: 76:2006+A1:2017 Rolling bearings - static load ratings, 2017a.

ISO: 15243:2017 Rolling bearings - damage and failures - terms, characteristics and causes, 2017b.

Jackson, R. and Green, I.: A finite element study of elasto-plastic hemispherical contact against a rigid flat, Journal of Tribology ASME, https://doi.org/10.1115/1.1866166, 2005.

Jain, S. and Hunt, H.: A dynamic model to predict the occurrence of skidding in wind-turbine bearings, Journal of Physics: Conference
5   Series, 305, https://doi.org/10.1088/1742-6596/305/1/012027, 2011.

Jiang, Z., Xing, Y., Guo, Y., Moan, T., and Gao, Z.: Long-term contact fatigue analysis of a planetary bearing in a land-based wind turbine drivetrain, 18, 591–611, https://doi.org/10.1002/we.1713, 2015.

Keller, J., Shend, S., Cotrell, J., and Greco, A.: Wind turbine drivetrain reliability collaborative workshop: a recap, Tech. rep., U.S. Department of Energy, https://www.researchgate.net/publication/307511892, 2016.

10   Kelley, N. D., Jonkman, B. J., Scott, G. N., Bialasiewicz, J., and Redmond, L. S.: The impact of coherent turbulence on wind turbine aeroelastic response and its simulation, American Wind Energy Association WindPower 2005 Conference and Exhibition, p. 17, 2005.

Kotzalas, M. N. and Doll, G. L.: Tribological advancements for reliable wind turbine performance, Philosophical Transactions of the Royal Society A: Mathematical, Physical and Engineering Sciences, 368, 4829–4850, https://doi.org/10.1098/rsta.2010.0194, http://rsta.royalsocietypublishing.org/cgi/doi/10.1098/rsta.2010.0194, 2010.

15   Lai, J. and Stadler, K.: Investigation on the mechanisms of white etching crack (WEC) formation in rolling contact fatigue and identification of a root cause for bearing premature failure, Wear, 364-365, 244–256, https://doi.org/10.1016/j.wear.2016.08.001, http://dx.doi.org/10.1016/j.wear.2016.08.001, 2016.

Liang, Y., An, Z., and Liu, B.: Fatigue life prediction for wind turbine main shaft bearings, 2013 International Conference on Quality, Reliability, Risk, Maintenance, and Safety Engineering (QR2MSE), pp. 888–893, https://doi.org/10.1109/QR2MSE.2013.6625711, 2013.

20   Liebherr: Main bearings for wind turbines - https://www.liebherr.com/en/gbr/products/components/large-diameter-bearing/main-bearings-for-wind-turbines/main-bearings-for-wind-turbines.html accessed 30/01/2019, https://www.liebherr.com/en/gbr/products/components/large-diameter-bearing/main-bearings-for-wind-turbines/main-bearings-for-wind-turbines.html.

Lugt, P.: Modern advancements in lubricating grease technology, Tribology International, 97, 467–477, 2016.

Mann, J.: Wind field simulation, Probabilistic Engineering Mechanics, 13, 269–282, https://doi.org/10.1016/S0266-8920(97)00036-2, http://
25   //linkinghub.elsevier.com/retrieve/pii/S0266892097000362, 1998.

Micallef, D. and Sant, T.: Turbine wake dynamics - chapter 2, https://doi.org/10.5772/63445, http://dx.doi.org/10.5772/63445, 2016.

Nelias, D. and Ville, F.: Detrimental effects of debris dents on rolling contact fatigue, Journal of Tribology, 122, 55–64, 1999.

Nilsson, R., Dwyer-Joyce, R. S., and Olofsson, U.: Abrasive wear of rolling bearings by lubricant borne particles, Proceedings of the Institution of Mechanical Engineers, Part J: Journal of Engineering Tribology, 220, 429–439, https://doi.org/10.1243/13506501J00205,
30   2006.

Novaes Menezes, E. J., Araújo, A. M., and Bouchonneau da Silva, N. S.: A review on wind turbine control and its associated methods, Journal of Cleaner Production, 174, 945–953, https://doi.org/10.1016/j.jclepro.2017.10.297, 2018.

Polinder, H., van der Pijl, F. F. A., de Vilder, G.-J., and Tavner, P.: Comparison of direct-drive and geared generator concepts for wind turbines, IEEE International Conference on Electric Machines and Drives, 21, 543–550, https://doi.org/10.1109/TEC.2006.875476, 2005.

35   Qu, Y., Chen, C. Z., and Zhou, B.: Study on fault diagnosis of wind turbine main bearing based on finite element analysis and wavelet analysis, Advanced Materials Research, 308-310, 1264–1268, https://doi.org/10.4028/www.scientific.net/AMR.308-310.1264, https://www.scientific.net/AMR.308-310.1264, 2011.

Schaeffler: Rotor shaft products and solutions - https://www.schaeffler.de/content.schaeffler.de/en/products-and-solutions/industrial/industry_solutions/wind_sector_cluster/wind/rotor_shaft/index.jsp accessed 30/01/2019, https://www.schaeffler.de/content.schaeffler.de/en/products-and-solutions/industrial/industry{_}solutions/wind{_}sector{_}cluster/wind/rotor{_}shaft/index.jsp.

Scott, K., Infield, D., Barltrop, N., Coultate, J., and Shahaj, A.: Effects of extreme and transient loads on wind turbine drive trains, 50th AIAA Aerospace Sciences Meeting Including the New Horizons Forum and Aerospace Exposition, https://doi.org/10.2514/6.2012-1293, 2012.

Sethuraman, L., Guo, Y., and Sheng, S.: Main bearing dynamics in three point suspension drivetrains for wind turbines, American Wind Energy Association WindPower Conference and Exhibition, 2015.

SKF: Self-aligning bearing solutions - http://www.skf.com/uk/industry-solutions/wind-energy/applications/main-shaft/self-aligning-bearing-solutions.html accessed 30/01/2019, http://www.skf.com/uk/industry-solutions/wind-energy/applications/main-shaft/self-aligning-bearing-solutions.html.

Spinato, F., Tavner, P., van Bussel, G., and Koutoulakos, E.: Reliability of wind turbine subassemblies, IET Renewable Power Generation, 3, 387, https://doi.org/10.1109/RTC.2016.7543074, http://digital-library.theiet.org/content/journals/10.1049/iet-rpg.2008.0060, 2009.

Stander, J. N., Venter, G., and Kamper, M. J.: Review of direct-drive radial flux wind turbine generator mechanical design, Wind Energy, 15, 459–472, https://doi.org/10.1002/we.484, 2012.

Stevens, R. J. and Meneveau, C.: Flow structure and turbulence in wind farms, Annual Review of Fluid Mechanics, 49, 311–39, https://doi.org/10.1146/annurev-fluid-010816-060206, 2017.

Stock, A.: Augmented control for flexible operation of wind turbines, Ph.D. thesis, University of Strathclyde, 2015.

Su, Y. S., Yu, S. R., Li, S. X., and He, Y. N.: Review of the damage mechanism in wind turbine gearbox bearings under rolling contact fatigue, Frontiers of Mechanical Engineering, pp. 1–8, https://doi.org/10.1007/s11465-018-0474-1, 2017.

Teng, W., Jiang, R., Ding, X., Liu, Y., and Ma, Z.: Detection and quantization of bearing fault in direct drive wind turbine via comparative analysis, Shock and Vibration, 2016, https://doi.org/10.1155/2016/2378435, 2016.

Terrell, E. J., Needelman, W. M., and Kyle, J. P.: Wind turbine tribology, Green Energy and Technology - Chapter 18,, pp. 483–530, https://doi.org/10.1007/978-3-642-23681-5, 2012.

Tong, V.-C. and Hong, S.-W.: Characteristics of tapered roller bearing subjected to combined radial and moment loads, International Journal of Precision Engineering and Manufacturing - Green Technology, 1, 323, https://doi.org/10.1007/s40684-014-0040-1, 2014.

Wang, J., Peng, Y., Qiao, W., and Hudgins, J. L.: Bearing fault diagnosis of direct-drive wind turbines using multiscale filtering spectrum, IEEE Transactions on Industry Applications, 53, 3029–3038, https://doi.org/10.1109/TIA.2017.2650142, 2017.

Wilkinson, M., Harman, K., Spinato, F., Hendriks, B., and Van Delft, T.: Measuring wind turbine reliability - results of the reliawind project, Proc. Eur. Wind Energy Conf. Brussels, 2011.

Wind Europe: Wind in power, Tech. rep., https://doi.org/10.1016/j.preghy.2016.08.046, http://www.ewea.org/fileadmin/ewea{_}documents/documents/publications/statistics/Stats{_}2011.pdf, 2017.

Yagi, S.: Bearings for wind turbines, Tech. Rep. 71, NTN, 2004.

Yagi, S. and Ninoyu, N.: Technical trends in wind turbine bearings, Tech. Rep. 76, NTN, 2008.

Zeid, I. and Padovan, J.: Finite element modeling of rolling contact, Computers & Structures, 14, 163–170, 1981.

Zhang, Z.: Automatic fault prediction of wind turbine main bearing based on SCADA data and artificial neural network, Open Journal of Applied Sciences, 08, 211–225, https://doi.org/10.4236/ojapps.2018.86018, http://www.scirp.org/journal/doi.aspx?DOI=10.4236/ojapps.2018.86018, 2018.

Zheng, J., Ji, J., Yin, S., and Tong, V. C.: The load distribution of the main shaft bearing considering combined load and misalignment in a floating direct-drive wind turbine, E3S Web of Conferences, 64, https://doi.org/10.1051/e3sconf/20186407009, 2018.

Zimroz, R., Bartelmus, W., Barszcz, T., and Urbanek, J.: Wind turbine main bearing diagnosis - a proposal of data processing and decision making procedure under non stationary load condition, Key Engineering Materials, 518, 437–444,

5   https://doi.org/10.4028/www.scientific.net/KEM.518.437, http://www.scientific.net/KEM.518.437, 2012.